Investigation of fracture characteristics of titanium/CFRP hybrid composites through experimental and numerical methods

Aysun Guven Citir[a*], Serkan Toros[b,c] and Fahrettin Ozturk[a,c]

[a]Department of Mechanical Engineering, Ankara Yildirim Beyazit University, Türkiye
[b]Department of Mechanical Engineering, Nigde Omer Halisdemir University, Türkiye
[c]Turkish Aerospace Industries Inc., Ankara, Türkiye

A R T I C L E I N F O	A B S T R A C T
	In this study, the delamination resistance of carbon fiber reinforced polymers (CFRP) consolidated with titanium alloy at the interface between the metal and composite was investigated experimentally and numerically. End-notched flexure (ENF) tests were performed to assess the fracture toughness (G_{IIC}) for Mode II crack expansion of Ti6Al4V titanium alloy/CFRP composite parts. The EFN test is applied to Ti6Al4V-carbon fiber/low melt poly (aryl ether ketone) (CF/LM-PAEK) and Ti6Al4V-carbon fiber/poly (ether ketone ketone) (CF/PEKK) composites with the $[0°]_{24}$ stacking sequence of unidirectional (UD) fibers. Experimental results indicate that the LM-PAEK composites exhibited Mode II strain energy release rate values 27.64 % higher than those of the PEKK composites. The finite element simulation by LS-DYNA shows good correlations with the experimental results, with an average error of 5.44 % for the PEKK and 10.58 % for the LM-PAEK, respectively. © 2024Growing Science Ltd. All rights reserved.

1. Introduction

Carbon fiber reinforced polymers (CFRP) are commonly used in various industries such as aerospace, automotive, marine, and defense industries due to their high specific modulus and strength. Moreover, metal/CFRP hybrid composites give the opportunity to enhance the mechanical properties including impact resistance and damage tolerance of CFRP by combining metal alloys. Metal/CFRP hybrid composites have been used in different industries. For example, Vlot and Gunnik (2001) indicated that the fiber metal laminate (FML) structures, produced by stacking CFRP on thin metal sheets, has been employed effectively as a fuselage skin material for Airbus A380. Song et al. (2000) investigated improved impact behaviors of the glass/epoxy/metal hybrid tubes, which the metallic tubes externally covered with glass/epoxy composite. Feito (2012) studied aero engine fan blades made from CFRP bonded to titanium strips to improve impact skills. Morano et al. (2023) utilized a corrugated aluminum alloy base with a CFRP skin characterized by a square wave profile to produce metal/composite joints. The objective was to improve the strength and energy dissipation of the flanges corrugation by using the modified metal/composite hybrid structure. Zhu et al. (2020) studied the crashworthiness properties of aluminum/CFRP tubes in both quasi-static and dynamic loading conditions. They conducted numerical and experimental investigations to assess the performance of various hybrid configurations, with a specific emphasis on their suitability for large scale industrial production subjected to different loading situations. Fink et al. (2010) examined the performance of the combined CFRP laminates and titanium alloy sheets to enhance the mechanical joint efficiency, specifically for use in the spacecraft payload adaptor. However, combining dissimilar materials brings new problems compared to monolithic ones. Fracture or delamination stands out as a prominent failure mode in hybrid composites. For this reason, it is essential to understand the fracture mechanism at the interface of bonded joints involving materials of differing properties. The crack propagation is driven by different fracture modes where Mode I, Mode II and Mode III which are opening mode, sliding mode and tearing mode, respectively. In terms of Mode II interfacial fracture, some studies have been conducted towards the fracture behavior of the interface between the

metal and composites. Pan et al. (2021) analyzed the impact performance and damage modes of titanium-CF/PEEK hybrid composite. It was found that the main disadvantages of the hybrid metal/composite parts include interlaminar delamination in composites, plastic strain of titanium plates, subsequent delamination at the interface between the metal and composites, and shear fracture of composites.

Sharma and Velmurugan (2021) studied the impact and energy absorption mechanisms of Ti6Al4V/glass fiber reinforced polymers (GFRP) hybrid composites. In addition, aluminum alloy sheets were used with GFRP in different layups. The fracture behavior of these metal/composite hybrid parts was also evaluated. There are several studies focused on delamination damage at the interface between Titanium and CFRP composites, particularly in the context of drilling and cutting processes (An et al.,2021; Fu et al., 2022). An et al.(2021) conducted an investigation on open-hole CFRP/Titanium composites using tensile tests to determine the ultimate tensile strength. The interface between the CFRP/Ti tensile test samples was examined for delamination microcracks, primarily involving fiber resin debonding and resin cracking. Additionally, fatigue tests were performed, and load-deformation curves were obtained for the samples. Fu et al. (2022) studied the impact of the rake angle on the delamination of CFRP/Ti6Al4V composites during the cutting process. Furthermore, they introduced a new mechanical model to establish the relationship between the rake angle and delamination in hybrid composites. Some other investigations conducted on titanium alloys combined with composites regarding their low and high velocity impact properties (Cortes & Cantwell, 2007; Kazemi et al., 2021; Li et al., 2017; Sun et al., 2022).

Steel/CFRP hybrid composites continue to attract great attention from researchers. Yao et al. (2022) carried out experimental and numerical study on the resistance of co-cured steel/CFRP hybrid composites to interfacial fracture based on the different surface treatments and manufacturing processes to enhance the bonding between the metal and composite materials. Alabtah and Mahdi (2021) aimed to investigate how the type and orientation of fibers impact the Mode I and Mode II values of steel/fiber reinforced composite. The study encompassed various fiber types, such as glass fiber, carbon fiber and kevlar fiber. It was concluded that the type and sequence of fibers significantly influence the fracture characteristics of the metal and composite joints. Koord et al. (2023) investigated the influence of the temperature on the resistance of the steel/CFRP hybrid composites to fracture. Park et al. (2021) examined Mode I and Mode II characteristics of the CFRP hybrid composites combined with steel besides the U-shape drawing process.

Another mostly used hybrid structure is aluminum alloy/composite, which exhibits significantly enhanced mechanical properties over conventional materials. Moreira et al. (2022) performed Mode I and Mode II tests to investigate the interfacial fracture resistance of bi-material aluminium/CFRP adhesive bonded joints. Furthermore, to eliminate the problems related to the crack length monitoring, data reduction methods were developed for these joints and were validated. Bienias et al. (2017) developed a methodology for the enhanced beam theory applicable to CFRP and GFRP composites, aiming to calculate the critical fracture toughness. For the comparison purposes, CFRP and GFRP composites combined with 2024-T3 aluminium metal in tests. The ENF tests were conducted to validate the performed FEA by cohesive zone method (CZM). García-González et al. (2015) and O'Masta et al. (2015) evaluated the impact properties of the aluminum alloy combining with composites. There are also some other studies on the investigation of the fracture characteristics of the aluminum hybrid composites (Jesudoss et al., 2022; Qi et al., 2021; Sahoo et al., 2013).

The work presented in this study aimed to conduct FEA to model the fracture characteristics of titanium/CFRP hybrid composite subjected to Mode II loading. The rate of delamination growth of titanium/CFRP bonded interfaces subjected to Mode II loading was also experimentally investigated by the end-notched flexure (ENF) test. The adhesive strength of the two different prepreg resins including LM-PAEK and PEKK were investigated regarding the Mode II fracture energy. To observe the bonding and wetting capabilities of these prepreg resins, no additional adhesive was used between the titanium and CFRP hybrid composites. The numerical results of the hybrid composite specimens were compared with the experimental data.

2. Material and methods

2.1 Materials

In the present study, Ti6Al4V sheet was used to bond with UD/CFRP composite. Two different prepreg materials were considered for UD/CFRP composite. One of the materials is a UD carbon fiber reinforced PEKK (Cetex® TC1320 by Toray), and second one is a UD carbon fiber reinforced LM-PAEK (Cetex® TC1225 by Toray), both of which have a 34 % resin content by weight. The mechanical properties of Ti6Al4V and UD/CFRP composites, which were taken from their datasheets and the literature (Tan & Falzon 2016, Clarkson 2021) shown in **Table 1**. A 50 μm thick Polyimide bagging film (Airtech®Thermalimide RCBS) was used to obtain the initial crack for ENF test specimens.

Table 1. Material properties of Ti6Al4V and UD/CFRP composites.

Properties	Ti6Al4V	PEKK	LM-PAEK
Density (g/cm³)	4.43	1.3	1.3
Modulus (GPa)	E=113	E_{11}=135, E_{22}=E_{33}=10, G_{12}=G_{13}=G_{23}=5.2	E_{11}=135, E_{22}=E_{33}=10, G_{12}=G_{13}=G_{23}=4.3
Poisson's ratio	0.342	υ_{12}=υ_{13}=υ_{23}=0.3	υ_{12}=υ_{13}=υ_{23}=0.33
Tensile strength 0° (MPa)	-	XT=2410	XT=2410
Tensile strength 90° (MPa)	-	YT=86	YT=86
Shear strength (MPa)	-	SC=152	SC=152

2.2 Preparation of the hybrid composites

CF/LM-PAEK and CF/PEKK prepregs were layed up and cured in the range of 380-400°C by using different autoclave cure cycles. UD/CFRP composites consisted of unidirectional 0° lay-ups with 24 plies. Each ply has a thickness of 0.140 mm. Ti6Al4V sheets with a thickness of 1.2 mm were used to prepare hybrid composites. Firstly, Ti6Al4V sheets were treated by wet blasting. Aluminum oxide (Al_2O_3) abrasive particles, ranging in size from 28 to 70 μm (240 mesh), were projected onto the samples with water at a 30° angle for 20 seconds. The air pressure was set to 0.4 MPa, with a gap of 0.15 m between the nozzle and the samples. The Ti6Al4V sheets underwent a chemical cleaning process prior to bonding with the composites.
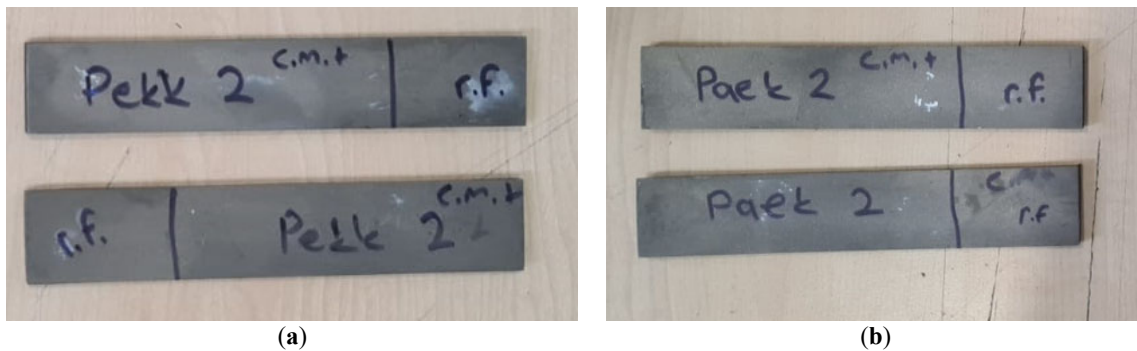

(**a**) (**b**)
Fig. 1. Test samples of titanium/UD carbon fiber reinforced with (**a**) PEKK matrix; (**b**) PAEK matrix.

Subsequently, the autoclave cure process was utilized for the one-step preparation of hybrid composites, facilitating the bonding of Ti6Al4V to UD/CFRP composite plates. An adhesive film was not used between the titanium alloy sheets and the prepreg layers. The bonding between the titanium sheets and the CFRP prepreg layers was achieved through the resin present in the CFRP prepreg during the autoclave cure process. To create a pre-crack notch, a release film with a width of 40 mm and thickness of 0.06 mm was applied at one edge of the hybrid composites in the Ti6Al4V/CFRP interface. The size of the ENF specimens were 140 mm x 25 mm for both Ti6Al4V and UD/CFRP composites, as illustrated in **Fig. 1**.

2.3 Mode II - End-Notched Flexure (ENF) test

End-notched flexure tests, carried out in accordance with the ASTM D7905 standard (ASTM, 2014), were employed to assess the Mode II interfacial fracture energy of metal/CFRP hybrid composites including the Ti6Al4V/unidirectional CF/LM-PAEK and Ti6Al4V/unidirectional CF/PEKK hybrid composites. The ENF test was conducted using a Shimadzu AGS-X 100 kN universal testing machine under the crosshead speed of 2 mm/min at room temperature (RT). The schematic representation of the Ti6Al4V/CFRP hybrid composites shown in **Fig. 2**. In addition, the geometrical parameters of the ENF test specimens used in the experiments were given in **Table 2**.
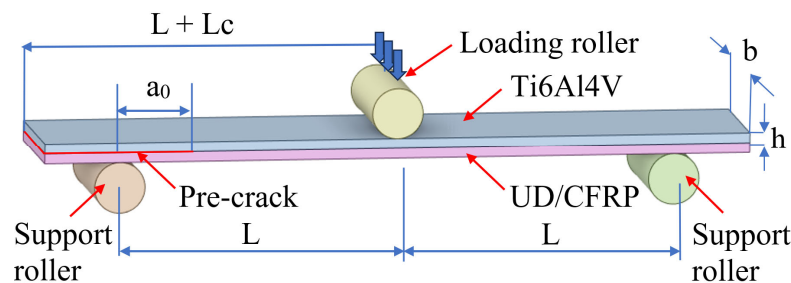
Fig. 2. Schematic representation of the ENF test.

The Mode II critical strain energy release rate (G_{IIC}) was determined by measuring the load and displacement values. Eq. (1) describes the flexural modulus while Eq. (2) and Eq. (3) define the Mode II energy release rate, derived from the simple beam theory (SBT) (Al-Khudairi et al., 2015; Brunner et al., 2013).

$$E_f = \frac{2L^3 + 3a_0^3}{8Bh_1^3C} \tag{1}$$

$$G_{II} = \frac{9a_0^2 P_C^2}{16B^2 E_f h_1^3} \tag{2}$$

$$G_{IIC} = \frac{3mP^2_{max}a^2_0}{2B} \tag{3}$$

wherein, width, half of the thickness, span length and crack length of the specimen denoted by B, h_1, L and a_0. In addition, P_C and δ_C are defined as the load and the bending displacement at the crack occurrence, respectively.

Table 2. Geometrical parameters of ENF test samples

Length between force and support, L, (mm)	50
Total length of the sample, l, (mm)	140
Width of the sample, b, (mm)	25
Total thickness of the sample, h, (mm)	4.56
Titanium sheet thickness, (mm)	1.2
UD/CFRP thickness, (mm)	3.36
Delamination length, a_0, (mm)	20
Distance from the center of the support roller to the cracked end of the specimen, Lc, (mm)	20

2.4 DSC experiments

To evaluate the poylmer degradation during the manufacturing process with a multiple heating cycles of the LM-PAEK and the PEKK samples, the degree of crystallinity of the LM-PAEK and the PEKK were investigated by means of a differential scanning calorimeter from Hitachi High-Tech Science (DSC 7020). After the ENF test, DSC samples were obtained by scraping the polymers from random locations along the surfaces of the composite cracks. The specimens of LM-PAEK and PEKK (between 5-10 mg) were analysed at a heating-cooling-heating cycle of 10 °C/min, in the temperature range of 55-380 °C in a Nitrogen atmosphere. From the second heating curve, the degree of crystallinity of the samples were calculated by Eq. (4) (Gray, 1970; Kong & Hay, 2002; Richardson, 1972).

$$X_C(\%) = \Delta H_f / \Delta H_f^0 \, x \, 100 \tag{4}$$

where ΔH_f is the enthalpy of fusion at the melting point is determined by calculating the area under the endothermic melting peak during the second heating cycle. Moreover, ΔH_f^0 is the melting enthalpy of fully crystallized polymers (130 J/g for LM-PAEK (Audoit et al., 2019) and 130 J/g for PEKK (Quiroga Cortés et al., 2016)).

2.5 Roughness and morphological characterization

The surface roughness of the ENF test samples were measured by the Mitutoyo SJ-301surface roughness tester. Each tracing has a 4 mm cutoff length. For each test sample, three surface roughness values were measured, and then mean average surface roughness (R_a) values were determined. To evaluate the morphological properties, the bonding surfaces of Ti6Al4V/LM-PAEK and Ti6Al4V/PEKK specimens after the ENF test were visually observed by optical microscopy using a Leica EZ4W stereo microscope (Leica Microsystems, Milton Keynes, UK).

3. Numerical simulation

In order to validate the FEA modeling methodology with the experimental ENF tests, we replicated the experimental setup by creating a composite with 24 layers, combined with a titanium sheet coupon.
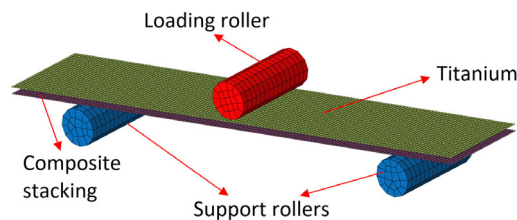
Fig. 3. Numerical simulation model of the ENF test specimens.

The composite had the same orientations and material properties as those shown in the experimental setup, and it was modeled using LS-DYNA finite element software. The critical strain energy release rate of Mode II, as well as the fracture behavior of the hybrid composites, was determined through the FEM analysis. **Fig. 3** illustrates the numerical simulation model of the ENF test.

3.1 Material model

The CFRP composites were modeled as an orthotropic material. The material parameters of Ti6Al4V and CFRP composites in the simulations were the same as the experiments shown in **Table 1**. In order to model the plastic deformation behavior of the Ti6Al4V sheets, MAT98_SIMPLIFIED_ JOHNSON_COOK material model card was used, and the related model constants were listed in **Table 3**.

Table 3. The simplified Johnson-Cook model constants of Ti6Al4V (Lesuer, 2000).

Material	A(MPa)	B(MPa)	n	C
Ti6Al4V	1098	1092	0.93	0.014

MAT54/55_ENHANCED_COMPOSITE_ DAMAGE model card was used for the modelling of the composite parts. A fully integrated shell element formulation (ELFORM:16) was defined for both the composites and titanium sheets. Furthermore, PART_COMPOSITE_LONG was chosen to define each shell ply with the desired ply direction, thickness, material properties and the element formulation for the CFRP composites. The loading roller and support rollers were modelled by using the MAT_RIGID material card and the solid elements.

3.2 Mesh model

The FE mesh size was generated with an element size of 1 mm for both titanium and CFRP parts then the mesh sensitivity study performed. The total number of elements in the FE model for each titanium and CFRP parts were 3500 for both PEKK and LM-PAEK materials. Element deletion was only allowed when the material fails mechanically. ERODE was defined as 0 in CONTROL _TIMESTEP card to prevent element deletions that may occur due to the time step reduction.

3.3 Contact definition

Instead of creating interlaminar cohesive element layers between the CFRP layers to bond the layers, CONTACT_AUTOMATIC_SURFACE_TO_SURFACE_TIEBREAK LS-DYNA card was used to create a tiebreak contact between CFRP composite layers. Additionally, pre-crack areas were simulated at the initial part between the composite and titanium structures using a separate mesh.

4. Result and discussion

4.1 Mode II - End-Notched Flexure test results

The average load-displacement curves of the ENF tests for titanium/CFRP hybrid composites shown in **Fig. 4**. For each specimen, the load increased linearly until reaching the peak value, after which it decreased due to the propagation of cracks at the critical load.
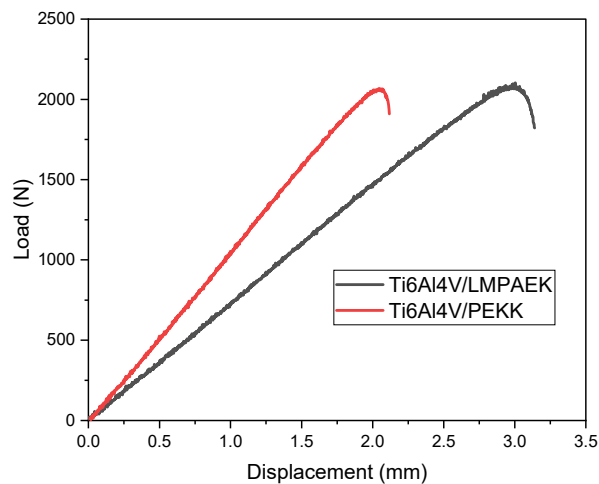
Fig. 4. Load-displacement curves determined from the experimental ENF tests.

According to the test results, the maximum load point values were found as 2094 N and 2069 N at the maximum displacement values of 3.08 mm and 2.44 mm for the Ti6Al4V/LM-PAEK and the Ti6Al4V/PEKK, respectively. The view of two of the Ti6Al4V/LM-PAEK and the Ti6Al4V/PEKK specimens after the ENF test from the top and the side shown in **Fig. 5.** It is visible that the test sample produced from the LM-PAEK composite had a higher adhesion ability with Ti6Al4V.

Fig. 5. The front view of the specimens after ENF test

Utilizing the load-displacement data, the average Mode-II strain energy release rates (G_{IIC}) of the specimens were calculated and are presented in Figure 6. The average G_{IIC} for Ti6Al4V/LM-PAEK was 1.667 kJ/m^2 while it was 1.306 kJ/m^2 for Ti6Al4V/PEKK. Therefore, Ti6Al4V/LM-PAEK had higher G_{IIC} values compared to Ti6Al4V/PEKK. The adhesive behavior of the titanium/CFRP was affected by the epoxy resins in the CFRP prepregs. It shows that the matrix material of the composites has an effect on the G_{IIC} values of titanium/CFRP composites.

The critical fracture toughness values of LM-PAEK and PEKK, which was taken from the product data sheet, were 2.6 kJ/m^2 and 2.3 kJ/m^2, respectively. The G_{IIC} values of Ti6Al4V/PEKK and Ti6Al4V/LM-PAEK are lower than those of the PEKK and the LM-PAEK composites. Additionally, other studies, including those involving steel/CFRP and titanium/CFRP, have demonstrated a decrease in interfacial fracture toughness for hybrid interfaces compared to monolithic interfaces (Koord et al., 2023). However, in this study, as no additional adhesive was used, the G_{IIC} values of titanium/CFRP hybrid composites were lower than the 3.70 kJ/m² determined in a previous study (J. Wang et al., 2023). G_{IIC} values can be influenced by various factors, including the type of metal material, adhesive used, or the combining process of hybrid structures, as indicated by another investigation. For instance, Titanium CP40 grade 2 combined with UD/PEKK using adhesive showed the G_{IIC} value of around 1.48 kJ/m² for a 25 mm delamination length (Adamos et al., 2020).
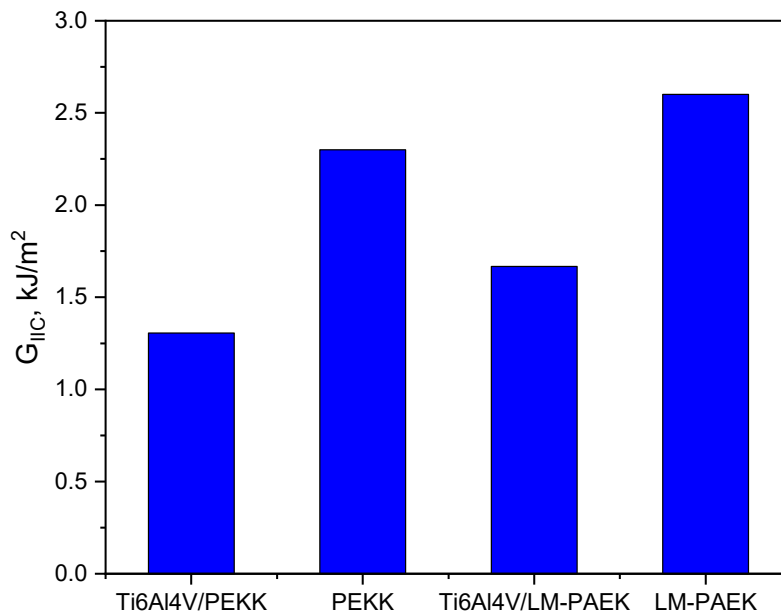

**Fig. 6.** Calculated the GIIC values of the Ti6Al4V/CFRP hybrid composites.

4.2 DSC measurements

The DSC thermograms of the second heating cycles for the LM-PAEK and the PEKK composites shown in Figure 7. The first heating cycle was not analyzed as it exhibits the thermal history of the polymers. Therefore, the first heating cycle only used to eliminate its effect by heating above polymers melting temperatures. The DSC thermograms of the second heating cycles for both polymers exhibit a smooth glass transition change and a significant endothermic melting peak. The parameters determined from the analysis of the curves were reported in **Table 4**.

Table 4. Crystallinity properties of LM-PAEK and PEKK polymers.

| Material	Glass transition temperature (°C)	Melting peak		Crystallinity (%)
		Temp (°C)	Enthalpy (J/g)	
LM-PAEK	143.3	305.8	7.50	5.76
PEKK	149.8	331.8	3.75	2.88

When comparing the LM-PAEK and the PEKK, it is clearly visible that the PEKK exhibits higher values of melting and glass transition temperatures than the LM-PAEK. On the other hand, the degree of crystallinity for the PEKK (2.88%) was lower than for the LM-PAEK (5.76%). The PEKK has lower crystallinity (< 6%) (W. Wang et al., 1997) compared to the LM-PAEK because the PEKK contains 67% ketone linkages, whereas the PEEK has 30%, which results in a slower crystallization kinetics (Ramaswamy et al., 2023). To clarify, for semi-crystalline polymers, the mobility of the amorphous chains is constrained by the presence of crystalline phases. As a result of this immobilization, there is an observed elevation in the glass transition temperature (Mano et al., 2005).
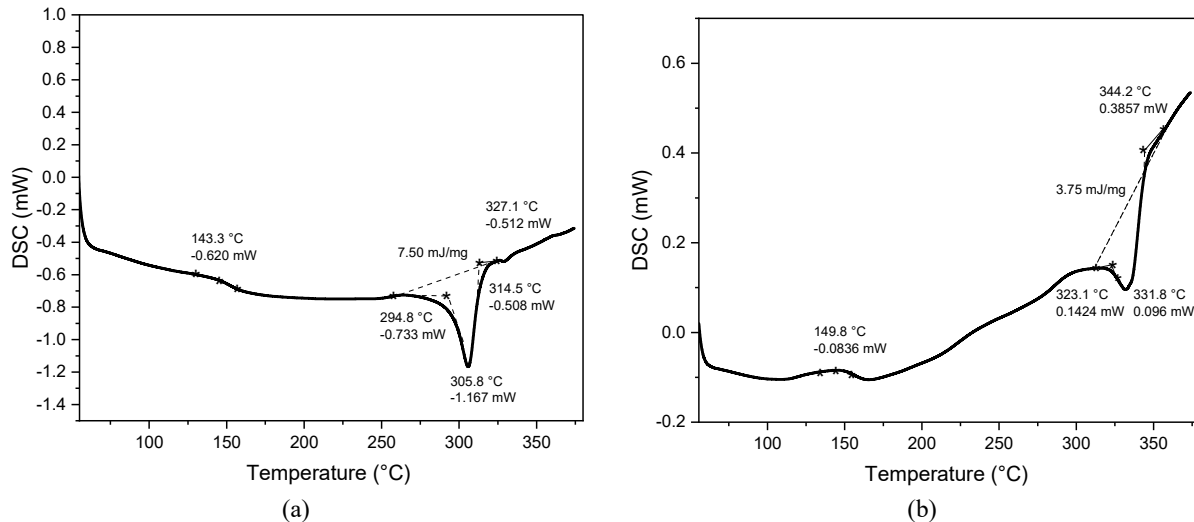
Fig. 7. DSC thermograms of the second heating cycle for (**a**) the LM-PAEK and (**b**) the PEKK samples.

## 4.3 Roughness and morphological characterization

The average surface roughness value of Ti6Al4V sheet was increased from 0.31 µm to 1.86 µm by wet blasting process. The mean R_a value of the LM-PAEK was 1.95 µm, while it was 1.90 µm for the PEKK. After the ENF tests, the mean R_a values were measured as 2.26 µm, 2.23 µm and 2.17 µm for LM-PAEK, PEKK, and Ti6Al4V, respectively. The bonding process simultaneously elevated the roughness of both the metal sheet and the composites as expected.
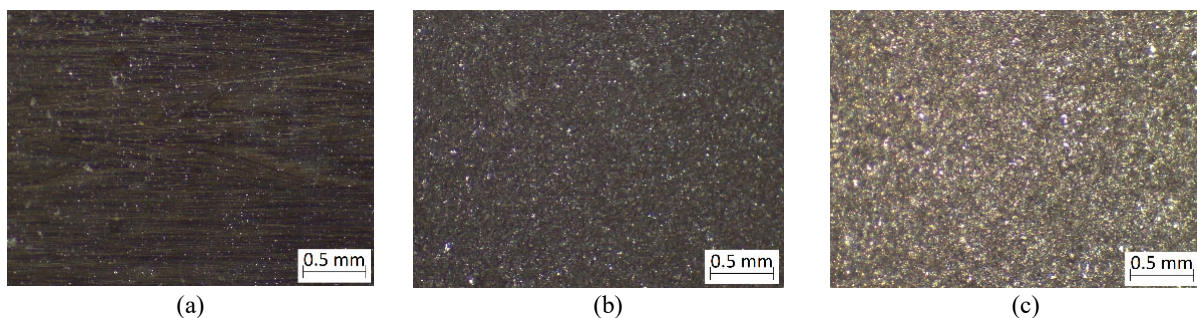
Fig. 8. Macrographs taken by stereomicroscope of (**a**) The PEKK surface before the ENF test; (**b**) The PEKK surface and (**c**) The Ti6Al4V surface after the ENF test.

The macrographs of all samples were taken between the metal/composite layer and some of these shown in **Fig. 8**. The surfaces of the PEKK sample before and after the ENF test were illustrated in **Fig. 8(a)** and **Fig. 8(b)**, respectively. The surface of the Ti6Al4V sample after the ENF test shown in **Fig. 8(c)**. Prior to the bonding process, the carbon fibers within the matrix could be seen clearly. However, after bonding, they became invisible as they were embedded in the matrix. In addition, the fracture surfaces of the titanium/CFRP hybrid composites after ENF test shown in **Fig. 9**.


(a)

(b)
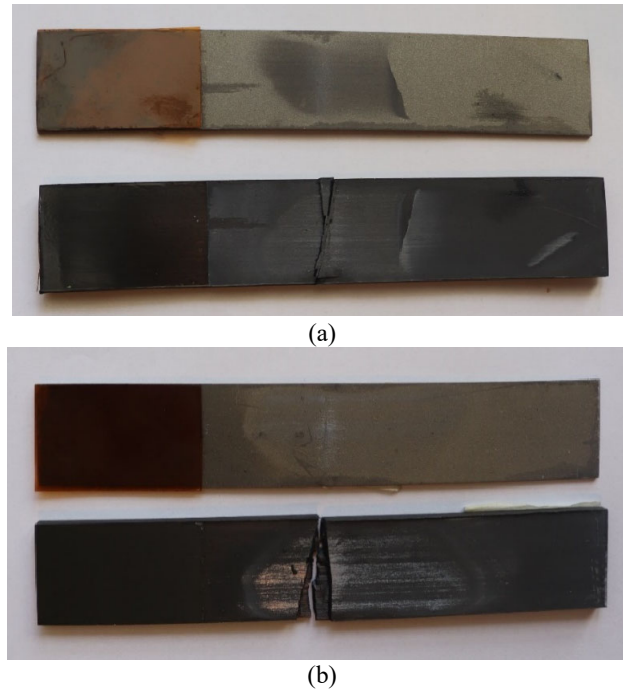
Fig. 9. Fracture surfaces of specimens after ENF test: (**a**) CF/LM-PAEK (**b**) CF/PEKK

4.4 Numerical results

In the solution part of the simulations, the reaction forces and the displacement values of the deformed structure were used to evaluate the deformed hybrid composite fracture behaviour and force-displacement graph. The finite element view of the deformed hybrid composite under the bending load, illustrated in **Fig. 10(a)** and **Fig. 11(a)**. As a result of the conducted numerical simulations, the maximum stress and crack path on the hybrid composites were also observed. Time-dependent displacement graphs of some randomly selected elements from the center of the composite plate model shown in **Fig. 10(b)** and **Fig. 11(b)**. As observed in the experiments, the fracture occurs at the similar displacement values in the analysis.

The comparison of the analysis results of the ENF tests and the average values of the experimental results shown in **Fig. 12**. The numerical results showed a lower load than the experimental results for all hybrid composites. This discrepancy may be attributed to the constant adhesive thickness maintained in the simulations. From the force-displacement curves of the numerical simulations of the PEKK and the LM-PAEK hybrid composites, the maximum critical loads were found as 1850 N at 1.91 mm and 1980 N at 2.77 mm, respectively. Based on both experimental and numerical simulation results, it is evident that LM-PAEK exhibits a superior adhesive behavior with titanium alloy. The average G_{IIC} values from the numerical results were found by using the load-displacement curve and Eq. (3) which is derived from the SBT. Therefore, the G_{IIC} values of numerical results were found as 0.9138 kJ/m^2 and 1.418 kJ/m^2 for the PEKK and the LM-PAEK hybrid composites, respectively.
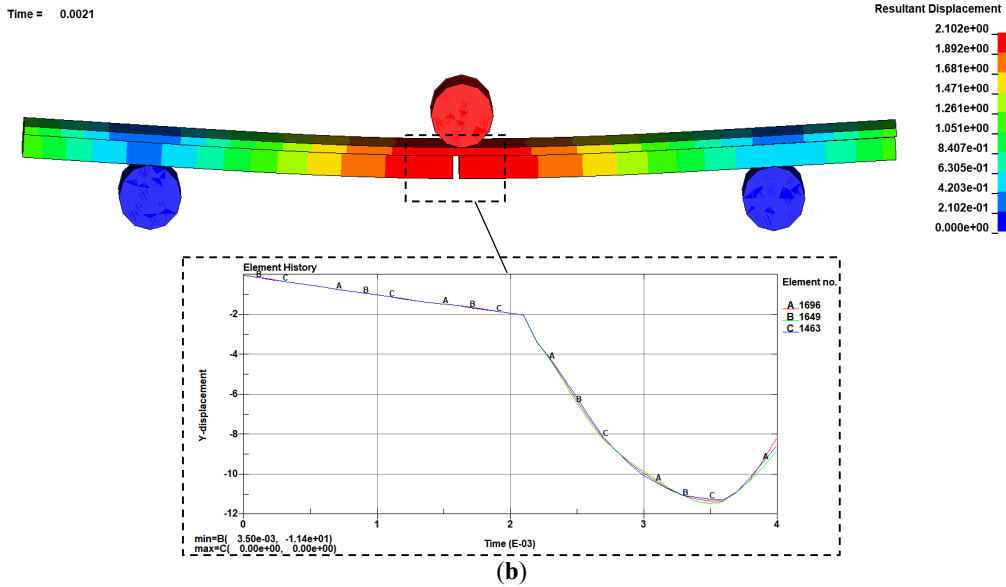

(**a**)

(b)
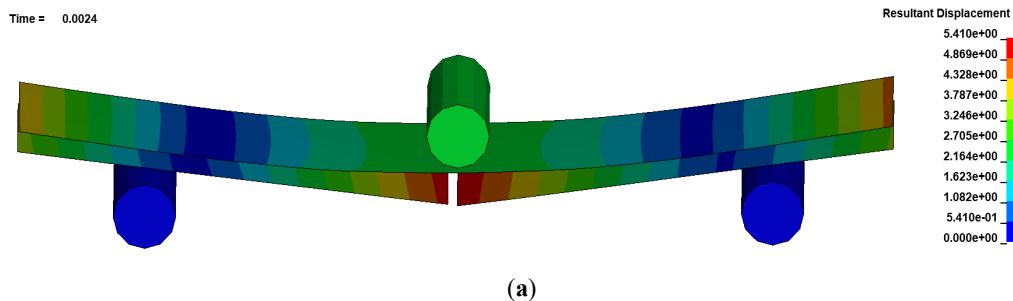
Fig. 10. Crack Mode II test for the Ti6Al4V/PEKK (**a**) Overview of the FEM results; (**b**) Displacement-time graphs of some selected damaged elements.
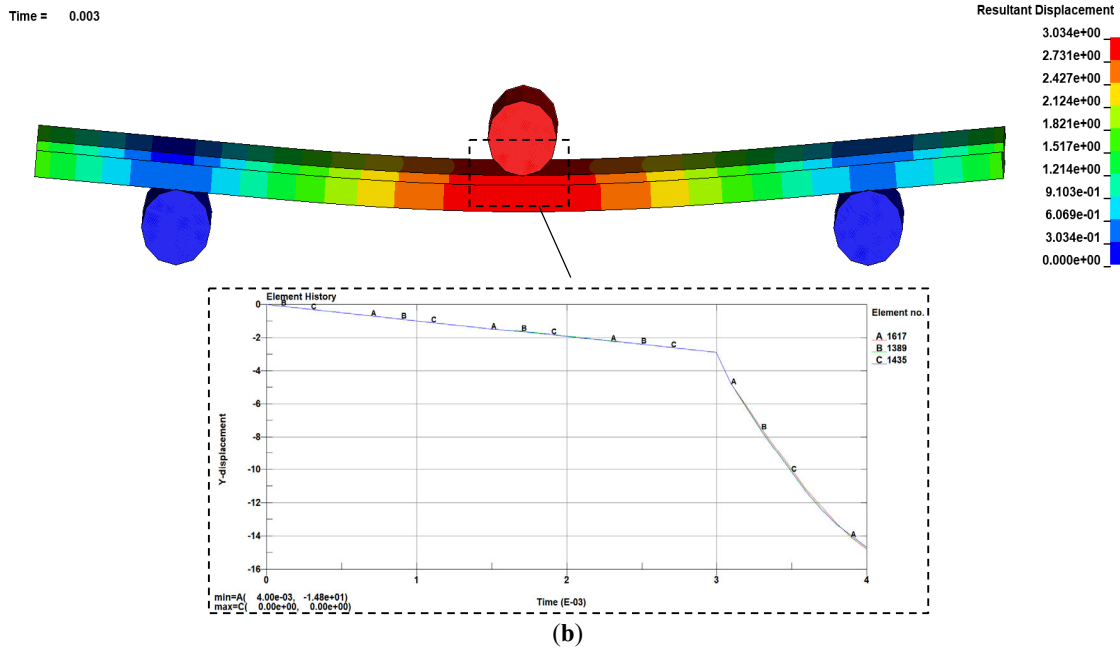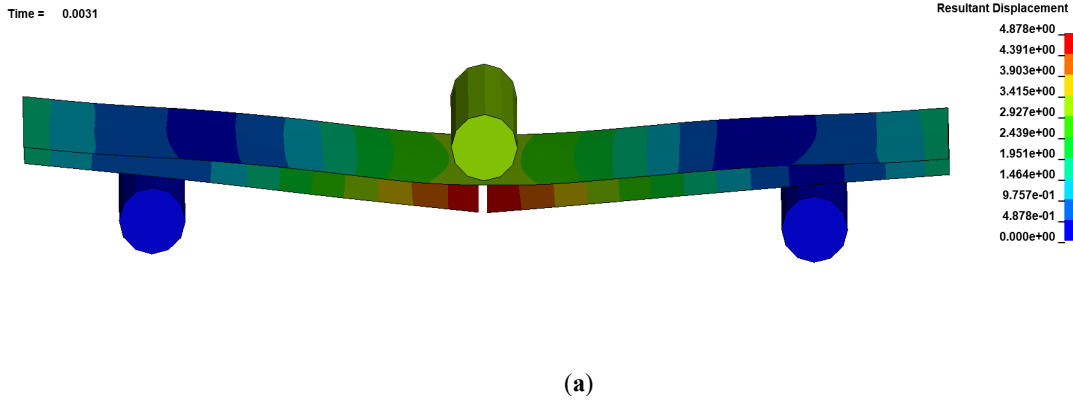

(a)

(b)

Fig. 11. Crack Mode II test for the Ti6Al4V/LM-PAEK (**a**) Overview of the FEM results;(**b**) Displacement-time graphs of some selected damaged elements.
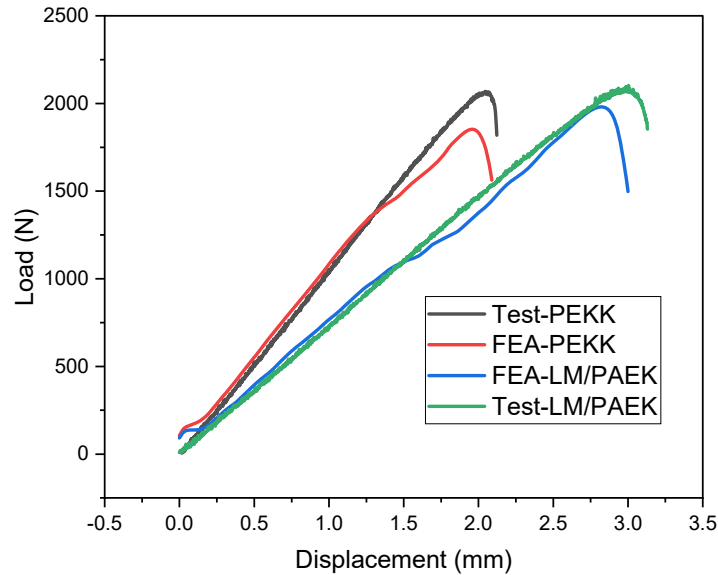
Fig. 12. Load vs. displacement - Experimental vs. the FEA for the hybrid composites.

5. Conclusions

In this research, the interfacial fracture toughness of the titanium/CFRP hybrid composites without any additional adhesive for two different matrices including the LM-PAEK and the PEKK were studied. Using the load-displacement curves derived from the ENF tests, the average G_{IIC} values were calculated for both titanium/CFRP hybrid composites. The joining of titanium sheet with the LM-PAEK composites shows higher interfacial fracture toughness than the PEKK composites. The Mode II critical strain energy release rate values of the Ti6Al4V/LM-PAEK are 27.64 % higher than the Ti6Al4V/PEKK determined by the ENF tests. Furthermore, the interfacial fracture toughness behavior of titanium/CFRP is predicted by an analysis model. Therefore, the G_{IIC} values for the LM-PAEK were found 55 % higher than the PEKK from numerical simulations. Furthermore, the numerical values show an average error of 5.44 % for the PEKK and 10.58 % for the LM-PAEK when compared to the experimental data. A strong concordance between the experimental results and the numerical results validates the accuracy of the FEA numerical models.

Acknowledgment

Declaration of interests

The author declares that they have no known competing financial interests or personal relationships could have appeared to influence the work reported in this paper.

References

Adamos, L., Tsokanas, P., & Loutas, T. (2020). An experimental study of the interfacial fracture behavior of Titanium/CFRP adhesive joints under mode I and mode II fatigue. *International Journal of Fatigue*, *136*, 105586.

Al-Khudairi, O., Hadavinia, H., Waggott, A., Lewis, E., & Little, C. (2015). Characterising mode I/mode II fatigue delamination growth in unidirectional fibre reinforced polymer laminates. *Materials & Design (1980-2015)*, *66*, 93-102.

Alabtah, F. G., & Mahdi, E. (2021). The effect of sizing optimization on the interface between high strength steel and fiber reinforced composite. *Composite Structures*, *266*, 113740.

Feito, D. A. (2012). Fracture mechanics of carbon fibre reinforced plastics to Ti-alloy adhesive joints. *Department of Mechanical Engineering*.

An, Q., Zhong, B., Wang, X., Zhang, H., Sun, X., & Chen, M. (2021). Effects of drilling strategies for CFRP/Ti stacks on static mechanical property and fatigue behavior of open-hole CFRP laminates. *Journal of Manufacturing Processes*, *64*, 409-420.

ASTM. (2014). ASTM D7905/D7905M-14: Standard Test Method for Determination of the Mode II Interlaminar Fracture Toughness of Unidirectional Fiber-Reinforced Polymer. *American Society for Testing and Materials*. https://doi.org/10.1520/D7905

Audoit, J., Rivière, L., Dandurand, J., Lonjon, A., Dantras, E., & Lacabanne, C. (2019). Thermal, mechanical and dielectric behaviour of poly (aryl ether ketone) with low melting temperature. *Journal of Thermal Analysis and Calorimetry*, *135*, 2147-2157.

Bieniaś, J., Dadej, K., & Surowska, B. (2017). Interlaminar fracture toughness of glass and carbon reinforced multidirectional fiber metal laminates. *Engineering Fracture Mechanics*, *175*, 127-145.

Brunner, A. J., Stelzer, S., Pinter, G., & Terrasi, G. P. (2013). Mode II fatigue delamination resistance of advanced fiber-reinforced polymer–matrix laminates: Towards the development of a standardized test procedure. *International journal of fatigue*, *50*, 57-62.

Clarkson, E. (2021). Medium Toughness PAEK thermoplastics Toray (Formerly TenCate) Cetex® TC1225 (LM PAEK) T700GC 12K T1E Unidirectional Tape 145 gsm 34% RC Material Allowables Statistical Analysis Report. *National Center for Advanced Materials Performance at Wichita State University, KS, USA*.

Cortes, P., & Cantwell, W. J. (2007). The impact properties of high-temperature fiber-metal laminates. *Journal of Composite Materials*, *41*(5), 613-632.

Fink, A., Camanho, P. P., Andrés, J. M., Pfeiffer, E., & Obst, A. (2010). Hybrid CFRP/titanium bolted joints: Performance assessment and application to a spacecraft payload adaptor. *Composites Science and Technology*, *70*(2), 305-317.

Fu, Q., Wu, S., Li, C., Xu, J., & Wang, D. (2022). Delamination and chip breaking mechanism of orthogonal cutting CFRP/Ti6Al4V composite. *Journal of Manufacturing Processes*, *73*, 183-196.

García-González, D., Rodríguez-Millán, M., Vaz-Romero, A., & Arias, A. (2015). High impact velocity on multi-layered composite of polyether ether ketone and aluminium. *Composite Interfaces*, *22*(8), 705-715.

Gray, A. P. (1970). Polymer crystallinity determinations by DSC. *Thermochimica Acta*, *1*(6), 563-579.

Hynes, N. R. J., Vignesh, N. J., Jappes, J. W., Velu, P. S., Barile, C., Ali, M. A., ... & Pruncu, C. I. (2022). Effect of stacking sequence of fibre metal laminates with carbon fibre reinforced composites on mechanical attributes: Numerical simulations and experimental validation. *Composites Science and Technology*, *221*, 109303.

Kazemi, M. E., Bodaghi, M., Shanmugam, L., Fotouhi, M., Yang, L., Zhang, W., & Yang, J. (2021). Developing thermoplastic hybrid titanium composite laminates (HTCLS) at room temperature: Low-velocity impact analyses. *Composites Part A: Applied Science and Manufacturing*, *149*, 106552.

Kong, Y., & Hay, J. N. (2002). The measurement of the crystallinity of polymers by DSC. *Polymer*, *43*(14), 3873-3878.

Koord, J., Völkerink, O., Petersen, E., & Hühne, C. (2023). Effect of low temperature on mode I and mode II interlaminar fracture toughness of CFRP-steel hybrid laminates. *Composites Part B: Engineering*, *262*, 110773.

Lesuer, D. (2000). *Experimental Investigations of Material Models for Ti-6Al-4V Titanium and 2024-T3 Aluminum*.

Li, X., Zhang, X., Zhang, H., Yang, J., Nia, A. B., & Chai, G. B. (2017). Mechanical behaviors of Ti/CFRP/Ti laminates with different surface treatments of titanium sheets. *Composite Structures*, *163*, 21-31.

Mano, J. F., Ribelles, J. G., Alves, N. M., & Sanchez, M. S. (2005). Glass transition dynamics and structural relaxation of PLLA studied by DSC: Influence of crystallinity. *Polymer*, *46*(19), 8258-8265.

O'masta, M. R., Compton, B. G., Gamble, E. A., Zok, F. W., Deshpande, V. S., & Wadley, H. N. G. (2015). Ballistic impact response of an UHMWPE fiber reinforced laminate encasing of an aluminum-alumina hybrid panel. *International Journal of Impact Engineering*, *86*, 131-144.

Morano, C., Wagih, A., Alfano, M., & Lubineau, G. (2023). Improving performance of composite/metal T-joints by using corrugated aluminum stiffeners. *Composite Structures*, *307*, 116652.

Moreira, R. D. F., de Moura, M. F. S. F., Silva, F. G. A., & Reina, J. P. A. (2022). Mixed-mode I+ II fatigue/fracture characterisation of bi-material Aluminium/CFRP bonded joints. *Composites Part B: Engineering*, *246*, 110240.

Pan, L., Yuan, X., Wang, M., Xue, P., Guo, H., Zhong, L., & Shi, H. (2021). Experimental and numerical simulation study on impact response of TC4/PEEK/Cf laminates under different mass impactors. *Composite Structures*, *258*, 113197.

Park, J. S., Kim, J. H., Park, J. H., & Ko, D. C. (2021). Prediction of the delamination at the steel and CFRP interface of hybrid composite part. *Materials*, *14*(21), 6285.

Qi, X., Wu, X., Gong, Y., Ning, H., Liu, F., Zou, R., ... & Hu, N. (2021). Interlaminar mechanical properties of nano-and short-aramid fiber reinforced glass fiber-aluminum laminates: a comparative study. *Journal of Materials Science*, *56*, 12198-12211.

Quiroga Cortés, L., Caussé, N., Dantras, E., Lonjon, A., & Lacabanne, C. (2016). Morphology   and dynamical mechanical properties of poly ether ketone ketone (PEKK) with meta phenyl links. *Journal of Applied Polymer Science*, *133*(19).

Ramaswamy, K., Modi, V., Rao, P. S., Martin, P. P., McCarthy, C. T., & O'Higgins, R. M. (2023). An investigation of the influence of matrix properties and fibre–matrix interface behaviour on the mechanical performance of carbon fibre-reinforced PEKK and PEEK composites. *Composites Part A: Applied Science and Manufacturing*, *165*, 107359.

Richardson, M. J. (1972). Precision differential calorimetry and the heat of fusion of polyethylene. In *Journal of Polymer Science Part C: Polymer Symposia* (Vol. 38, No. 1, pp. 251-259). New York: Wiley Subscription Services, Inc., A Wiley Company.

Sahoo, P. K., Dattaguru, B., Manjunatha, C. M., & Murthy, C. R. L. (2013). Strength prediction methods for adhesively bonded lap joints between composite–composite/metal adherends. *Advances in Modeling and Design of Adhesively Bonded Systems*, 219-236.

Sharma, A. P., Velmurugan, R., Shankar, K., & Ha, S. K. (2021). High-velocity impact response of titanium-based fiber metal laminates. Part I: experimental investigations. *International Journal of Impact Engineering*, *152*, 103845.

Song, H. W., Wan, Z. M., Xie, Z. M., & Du, X. W. (2000). Axial impact behavior and energy absorption efficiency of composite wrapped metal tubes. *International Journal of Impact Engineering*, *24*(4), 385-401.

Sun, J., Xu, S., Lu, G., Wang, Q., & Gong, A. (2022). Ballistic impact experiments of titanium-based carbon-fibre/epoxy laminates. *Thin-Walled Structures*, *179*, 109709.

Tan, W., & Falzon, B. G. (2016). Modelling the crush behaviour of thermoplastic composites. *Composites Science and Technology*, *134*, 57-71.

Vlot, A., & Gunnink, J. W. (Eds.). (2011). *Fibre metal laminates: an introduction*. Springer Science & Business Media.

Wang, J., Ding, H., Jiang, J., & Bi, Y. (2023). Experimental and numerical investigation on test methods for mode II fracture of composite-titanium adhesively bonded structures. *Fatigue & Fracture of Engineering Materials & Structures*, *46*(10), 3766-3787.

Wang, W., Schultz, J. M., & Hsiao, B. S. (1997). Dynamic study of crystallization-and melting-induced phase separation in PEEK/PEKK blends. *Macromolecules*, *30*(16), 4544-4550.

Yao, Y., Shi, P., Chen, M., Chen, G., Gao, C., Boisse, P., & Zhu, Y. (2022). Experimental and numerical study on Mode I and Mode II interfacial fracture toughness of co-cured steel-CFRP hybrid composites. *International Journal of Adhesion and Adhesives*, *112*, 103030.

Zhu, G., Liao, J., Sun, G., & Li, Q. (2020). Comparative study on metal/CFRP hybrid structures under static and dynamic loading. *International Journal of Impact Engineering*, *141*, 103509.